Nonlinear optical properties of induced transmission filters

Daniel T. Owens,[1] Canek Fuentes-Hernandez,[1] Joel M. Hales,[2] Joseph W. Perry[2] and Bernard Kippelen[1,*]

[1]*Center for Organic Photonics and Electronics, School of Electrical and Computer Engineering, Georgia Institute of Technology, Atlanta, GA 30332, USA*
[2]*Center for Organic Photonics and Electronics, School of Chemistry and Biochemistry, Georgia Institute of Technology, Atlanta, GA 30332, USA*
**kippelen@ece.gatech.edu*

Abstract: The nonlinear optical (NLO) properties of induced transmission filters (ITFs) based on Ag are experimentally determined using white light continuum pump-probe measurements. The experimental results are supported using simulations based on the matrix transfer method. The magnitude of the NLO response is shown to be 30 times that of an isolated Ag film of comparable thickness. The impacts of design variations on the linear and NLO response are simulated. It is shown that the design can be modified to enhance the NLO response of an ITF by a factor of 2 or more over a perfectly matched ITF structure.

OCIS codes: (190.4360) Nonlinear optics, devices; (190.4400) Nonlinear optics, materials; (190.7110) Ultrafast nonlinear optics

References and links

1. D. Ricard, P. Roussignol, and C. Flytzanis, "Surface-mediated enhancement of optical phase conjugation in metal colloids," Opt. Lett. **10**(10), 511–513 (1985).
2. K. Uchida, S. Kaneko, S. Omi, C. Hata, H. Tanji, Y. Asahara, A. J. Ikushima, T. Tokizaki, and A. Nakamura, "Optical nonlinearities of a high concentration of small metal particles dispersed in glass - copper and silver particles," J. Opt. Soc. Am. B **11**(7), 1236–1243 (1994).
3. H. B. Liao, R. F. Xiao, J. S. Fu, and G. K. L. Wong, "Large third-order nonlinear optical susceptibility of Au-Al2O3 composite films near the resonant frequency," Appl. Phys. B **65**(4-5), 673–676 (1997).
4. X. Zhang, H. Fang, S. Tang, and W. Ji, "Determination of two-photon-generated free-carrier lifetime in semiconductors by a single-beam Z-scan technique," Appl. Phys. B **65**(4-5), 549–554 (1997).
5. X. J. Zhang, W. Ji, and S. H. Tang, "Determination of optical nonlinearities and carrier lifetime in ZnO," J. Opt. Soc. Am. B **14**(8), 1951–1955 (1997).
6. J. H. Bechtel, and W. L. Smith, "2-photon absorption in semiconductors with picosecond laser pulses," Phys. Rev. B **13**(8), 3515–3522 (1976).
7. R. W. Boyd, *Nonlinear Optics* (Academic Press, San Diego, CA, 2003).
8. R. S. Bennink, Y. K. Yoon, R. W. Boyd, and J. E. Sipe, "Accessing the optical nonlinearity of metals with metal-dielectric photonic bandgap structures," Opt. Lett. **24**(20), 1416–1418 (1999).
9. M. Scalora, N. Mattiucci, G. D'Aguanno, M. Larciprete, and M. J. Bloemer, "Nonlinear pulse propagation in one-dimensional metal-dielectric multilayer stacks: ultrawide bandwidth optical limiting," Phys. Rev. E Stat. Nonlin. Soft Matter Phys. **73**(1), 016603 (2006).
10. G. D'Aguanno, N. Mattiucci, M. J. Bloemer, and M. Scalora, "Accessing quadratic nonlinearities of metals through metallodielectric photonic-band-gap structures," Phys. Rev. E Stat. Nonlin. Soft Matter Phys. **74**(3), 036605 (2006).
11. T. K. Lee, A. D. Bristow, J. Hubner, and H. M. van Driel, "Linear and nonlinear optical properties of Au-polymer metallodielectric Bragg stacks," J. Opt. Soc. Am. B **23**(10), 2142–2147 (2006).
12. G. J. Lee, Y. Lee, S. G. Jung, B. Y. Jung, C. K. Hwangbo, S. Kim, and I. Park, "Design, fabrication, linear and nonlinear optical properties of metal-dielectric photonic bandgap structures," J. Korean Phys. Soc. **51**(91), 431–437 (2007).
13. G. H. Ma, and S. H. Tang, "Ultrafast optical nonlinearity enhancement in metallodielectric multilayer stacks," Opt. Lett. **32**(23), 3435–3437 (2007).
14. T. Ergin, T. Benkert, H. Giessen, and M. Lippitz, "Ultrafast time-resolved spectroscopy of one-dimensional metal-dielectric photonic crystals," Phys. Rev. B **79**, 245134 (2009).
15. A. Husakou, and J. Herrmann, "Steplike transmission of light through a metal-dielectric multilayer structure due to an intensity-dependent sign of the effective dielectric constant," Phys. Rev. Lett. **99**(12), 127402 (2007).

#131590 - $15.00 USD Received 13 Jul 2010; revised 12 Aug 2010; accepted 14 Aug 2010; published 24 Aug 2010

16. P. H. Berning, and A. F. Turner, "Induced transmission in absorbing films applied to band pass filter design," J. Opt. Soc. Am. **47**(3), 230–239 (1957).
17. H. A. Macleod, *Thin-film optical filters* (Institute of Physics Publishing, Philadelphia, PA, 2001).
18. G. Q. Du, H. T. Jiang, Z. S. Wang, and H. Chen, "Optical nonlinearity enhancement in heterostructures with thick metallic film and truncated photonic crystals," Opt. Lett. **34**(5), 578–580 (2009).
19. P. W. Milonni, and J. H. Eberly, *Lasers* (John Wiley & Sons, USA, 1988).
20. D. T. Owens, C. Fuentes-Hernandez, J. M. Hales, J. W. Perry, and B. Kippelen, "A comprehensive analysis of the contributions to the nonlinear optical properties of thin Ag films," J. Appl. Phys. **107**(12), 123114 (2010).
21. G. L. Eesley, "Observation of non-equilibrium electron heating in copper," Phys. Rev. Lett. **51**(23), 2140–2143 (1983).
22. H. E. Elsayed-Ali, T. B. Norris, M. A. Pessot, and G. A. Mourou, "Time-resolved observation of electron-phonon relaxation in copper," Phys. Rev. Lett. **58**(12), 1212–1215 (1987).
23. R. W. Schoenlein, W. Z. Lin, J. G. Fujimoto, and G. L. Eesley, "Femtosecond studies of nonequilibrium electronic processes in metals," Phys. Rev. Lett. **58**(16), 1680–1683 (1987).
24. S. D. Brorson, A. Kazeroonian, J. S. Moodera, D. W. Face, T. K. Cheng, E. P. Ippen, M. S. Dresselhaus, and G. Dresselhaus, "Femtosecond room-temperature measurement of the electron-phonon coupling constant gamma in metallic superconductors," Phys. Rev. Lett. **64**(18), 2172–2175 (1990).
25. T. Tokizaki, A. Nakamura, S. Kaneko, K. Uchida, S. Omi, H. Tanji, and Y. Asahara, "Subpicosecond time response of third order optical nonlinearity of small copper particles in glass," Appl. Phys. Lett. **65**(8), 941–943 (1994).
26. T. S. Ahmadi, S. L. Logunov, and M. A. ElSayed, "Picosecond dynamics of colloidal gold nanoparticles," J. Phys. Chem. **100**(20), 8053–8056 (1996).
27. Y. Hamanaka, N. Hayashi, A. Nakamura, and S. Omi, "Ultrafast relaxation dynamics of electrons in silver nanocrystals embedded in glass," J. Lumin. **76–77**, 221–225 (1998).

1. Introduction

Metals are known to have some of the strongest nonlinear optical (NLO) responses of any material [1–3], orders of magnitude larger than typical dielectric or semiconductor materials [4–7]. This nonlinearity is not easily accessed, however, because a metal film of appreciable thickness is highly reflective and light that is not reflected is mostly absorbed. For this reason, bulk metal cannot be used to exploit its large NLO response and, consequently, metallic films with defined sub-structure must be created to access this nonlinearity given such limited interaction lengths. Recently there has been interest in the NLO properties of structures that contain continuous thin films of metal such as the metal-dielectric photonic band-gap (MDPBG) [8–15]. These structures make use of resonance to overcome reflection losses, thereby causing the light to tunnel through the metal films and giving direct access to the metal's nonlinearity.

The focus of this present work is on a structure similar to the MDPBG, namely the induced transmission filter (ITF). The ITF, originally described in 1957 [16], presents an interesting opportunity for NLO applications because it contains only a single metal layer; as such, it is a simpler structure to fabricate and analyze. The ITF is also interesting in its own right because, as will be shown, it is possible to amplify the NLO response of an isolated Ag film.

In this paper, we present the design and fabrication of an ITF having a peak linear transmittance of 63% and we discuss the experimental demonstration of an enhancement in its NLO response by a factor of 30 over an isolated Ag film. We have also modeled a series of ITFs in order to develop an understanding of how variations in structure impact the strength of the NLO response. In doing so, we have demonstrated the possibility of a further enhancement of the NLO response by a factor of 2.

The remainder of the paper is organized as follows. Section 2 presents a discussion of the conceptual understanding of the ITF design. Section 3 presents the fabrication, linear characterization, nonlinear characterization, and simulation procedures used in this work. Section 4 presents the experimental results of the linear and NLO characterization. Section 5 presents simulations of the NLO response for ITFs with different structural variations.

2. ITF design

For the purposes of this study, an ITF consists of a single metal layer and an adjoining dielectric structure that is designed to induce transmission through the metal layer. Two

#131590 - $15.00 USD Received 13 Jul 2010; revised 12 Aug 2010; accepted 14 Aug 2010; published 24 Aug 2010

variations of the ITF design are considered here: the single sided ITF and the double sided ITF, both shown in Fig. 1. The single sided ITF consists of a ¼ wave stack, a dielectric spacer, and a thin film of metal followed by a protective layer; the double sided ITF adds a second spacer and ¼ wave stack in place of the protective layer. In [16,17], the ITFs are double sided and the structure is symmetric; that is, the top spacer and ¼ wave stack are identical to the bottom ones. In [18], the ITFs are single sided and have no spacer layer. In the present study we focus on single sided ITFs and on double sided ITFs where the spacer thicknesses and number of periods in the ¼ wave stack differ from top to bottom.

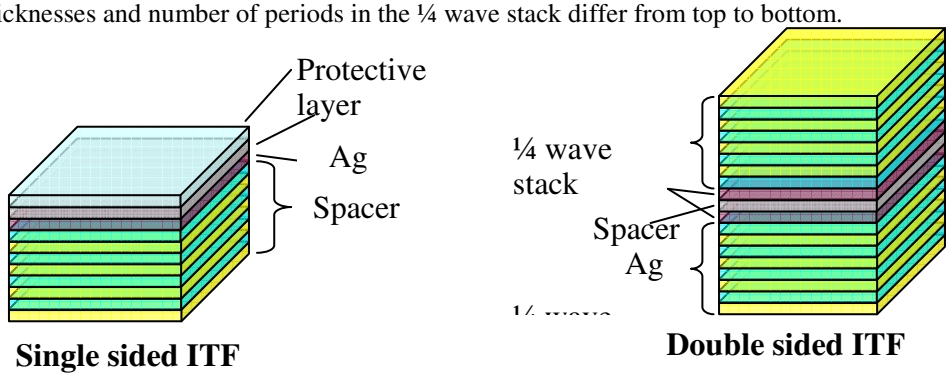

Fig. 1. Schematics of single sided and double sided ITFs.

These structural variations arise from different ways of conceptualizing ITFs. The ITF was originally conceived as a thick metal film with dielectric structures on each side that serve as antireflection coatings to the metal film [16,17]. Thick metal films are both highly absorbing and highly reflective. If the reflections can be eliminated, and the film can be made sufficiently thin, only a fraction of the incident light will be absorbed while the majority will be transmitted.

In [18], a structure was investigated that, while not called an ITF, is by the above definition a single sided ITF without a spacer layer. This structure was described as a heterostructure between a metal layer and a truncated photonic crystal, where the photonic crystal is the ¼ wave stack. It was theoretically shown that this structure displayed improved transmittance and significant field enhancement at the metal/dielectric interface at the target wavelength compared to an isolated metal film.

The method used in the present study considers a single sided ITF as a Fabry-Perot cavity where the Ag film is one mirror, albeit somewhat lossy, and the ¼ wave stack is the other. The remaining dielectric is the cavity spacer. In a high-finesse Fabry-Perot, where the total reflection at the peak wavelength is zero, two conditions must be met [19]. First, the reflectances of the two mirrors must be equal; second, the round-trip phase within the cavity must be an integer multiple of 2π. In the ideal ITF, the first condition is met by choosing the number of periods and the refractive indices of the ¼ wave stack such that its reflectance is equal to that of the Ag film. Alternatively, the thickness of the Ag film can be chosen to match the reflectance of the dielectric structure. The second condition is met by choosing the thickness of the spacer layer to compensate for the non-zero phase shift of the reflection off the Ag film and the dielectric interface.

#131590 - $15.00 USD Received 13 Jul 2010; revised 12 Aug 2010; accepted 14 Aug 2010; published 24 Aug 2010

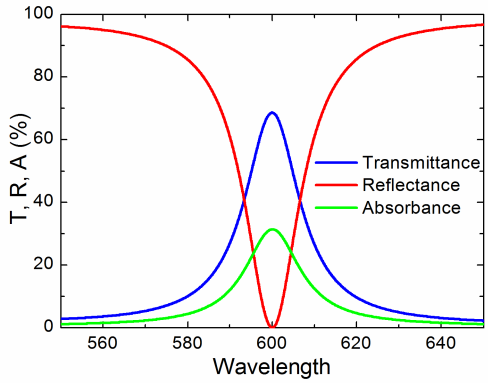

Fig. 2. Example simulated ITF transmittance, reflectance, and absorbance.

In this way the ITF can be designed to have zero, or near zero, reflectance at a specified wavelength. A simulation of this is shown in Fig. 2. This ITF has the structure

$$(HL)_x\ R\ Ag, \qquad (1)$$

where H and L represent the high and low index materials making up the ¼ wave stack with x = 4 periods designed to have a center wavelength λ = 600 nm, with refractive indices n_H = 2.109 and n_L = 1.5, and thicknesses of 71 nm and 100 nm, respectively. R represents a spacer layer with thickness 73.6 nm, and Ag represents an Ag film with thickness 30 nm. This design methodology forms the foundation of the structures that are fabricated and simulated in the following sections.

3. Experimental procedure

3.1 Fabrication

All samples were fabricated on 0.16 mm-thick glass cover slips that had been cleaned ultrasonically in deionized water, acetone, and isopropanol for 15 minutes each. Ta_2O_5 and SiO_2 were used as the high and low index materials in the ¼ wave stack, with layer thicknesses on the order of 70 to 100 nm. SiO_2 was also used as the spacer layer and protective layer. A 0.25 nm layer of Ti was used as an adhesion layer between SiO_2 and Ag. The films were deposited with a Kurt J. Lesker Axxis electron beam deposition system with a starting pressure of 1.3×10^{-6} Pa. The Ag, SiO_2, and Ta_2O_5 layers were deposited at a rate of 0.2 nm/s and the Ti layers at a rate of 0.025 nm/s. The samples were actively cooled and held at room temperature throughout the deposition. After each Ta_2O_5 layer the structure was removed from the deposition chamber and annealed at 200° C for on hour in air in order to restore any oxygen that may have dissociated from the Ta_2O_5 during the deposition process.

3.2 Linear optical characterization

The refractive indices of the dielectric materials were measured using a J. A. Woollam M2000 spectroscopic ellipsometer with a 50 nm layer of each material deposited on separate Si wafers cleaned in the same manner as the glass cover slips described above; furthermore, the same annealing procedures were used on the Ta_2O_5 films.

The linear optical properties of the samples were characterized using a combination of transmittance and reflectance measurements at normal incidence. Transmission measurements were made using a Cary 5E UV/Vis/NIR spectrophotometer and reflection measurements were made using a Xenon light source and a monochromator, where detection of the signal and reference was accomplished by a pair of Si photodiodes connected to lock-in amplifiers. The standard sample used for reflection measurements was a 160 nm-thick Ag film covered by 50 nm of SiO_2, and the measurements were corrected to account for the fact that the reflectance of the standard was not exactly 100%. The correction factor was calculated using

#131590 - $15.00 USD Received 13 Jul 2010; revised 12 Aug 2010; accepted 14 Aug 2010; published 24 Aug 2010

the matrix transfer method applied to this structure, assuming a bulk refractive index for Ag. This resulted in the reflection data being adjusted upwards by 1-2% across the visible portion of the spectrum.

3.3 Nonlinear optical characterization

The NLO properties of the structures were characterized using a commercially available white-light continuum pump-probe spectroscopy system (Helios, Ultrafast Systems) with a procedure described elsewhere [20]. The pump wavelength was 600 nm and the probe covered the wavelength range from 500 to 700 nm. The pump fluence used was 32 J/m^2 and the probe had fluence less than 0.3 J/m^2 in the pass band of the measured structures. All measurements were taken at normal incidence.

3.4 Simulation procedure

The linear and NLO properties were simulated over time using a procedure based on the matrix transfer method. First, the linear optical transmittance, reflectance and absorbance were calculated using the matrix transfer method where the complex permittivity of Ag was represented by the Drude model:

$$\varepsilon = \varepsilon_\infty - \frac{\omega_p^2}{\omega^2 + i\left(\gamma + \beta\omega^2\right)\omega}, \tag{2}$$

where ε_∞ is the sum of the interband contributions, ω_p is the bulk plasma frequency, γ is a frequency independent damping parameter, and β is a frequency dependent damping parameter. The values of each of these parameters were extracted from the linear optical measurements of a 30 nm thick Ag film.

The NLO properties were simulated assuming the NLO response of Ag is a function primarily of the electron temperature, and the maximum NLO response occurs when the electron temperature is at its peak. This occurs, ignoring electron thermalization, at the tail end of the optical excitation pulse before the electrons have lost much of their heat to the lattice. The NLO response was simulated at this one moment in time.

The peak electron temperature was calculated assuming all of the energy absorbed by the structure was converted directly to heat in the electron cloud of the metal film. The electron temperature was calculated based on the temperature dependent specific heat of the electron cloud:

$$C_e\left(T_e\right)\frac{dT_e}{dt} = P\left(t\right), \tag{3}$$

where

$$C_e(T_e) = 65T_e \ \left[\mathrm{J/m^3K}\right] \tag{4}$$

is the temperature dependent volumetric specific heat,

$$P\left(t\right) = \frac{aI\left(t\right)}{d} \ \left[\mathrm{W/m^3}\right] \tag{5}$$

is the absorbed power as a function of time, $I(t)$ [W/m^2] is the irradiance at the center of the pump as a function of time, a is the fraction of power absorbed by the Ag film, and d is the thickness of the Ag film. Integrating Eq. (3) and solving for the peak electron temperature (assuming pre-excitation T_e = 300 K) gives

$$T_e = \sqrt{\frac{2aF}{65d} + 300^2}, \tag{6}$$

#131590 - $15.00 USD Received 13 Jul 2010; revised 12 Aug 2010; accepted 14 Aug 2010; published 24 Aug 2010

where $F = \int I(t)$ is the fluence at the peak of the pump pulse.

The measured temperature dependence of the Drude model parameters was then used to recalculate the complex permittivity of Ag at the point in time when all of the pulse energy has been absorbed by the electron cloud, before it is transferred to the lattice. The transmittance, reflectance, and absorbance of the structure were then calculated using the modified complex permittivity of Ag, and the changes in transmittance and reflectance were extracted.

This simulation process was compared to the iterative numerical processes such as those used in [20]. A small amount of error is introduced because the absorbance of the Ag film would increase slightly as it heats up. However, this error was determined to be no more than a few percent of the simulated change so is disregarded here.

4. Experiment

In order to demonstrate the NLO response of an ITF we fabricated two single sided ITFs with the structure

$$G\ (HL)_x\ R\ Ag\ P, \qquad (7)$$

where G represents the glass substrate; H and L represent a ¼ wave layer of the high index and low index materials, in this case Ta_2O_5 and SiO_2, respectively; R represents a spacer layer of 75 nm SiO_2; Ag represents a 30 nm layer of Ag; and P represents a 410 nm protective coating of SiO_2. The parameter x defines the number of periods in the ¼ wave stack; for ITF 1, $x = 5$, and for ITF 2, $x = 4$. This is the only difference between the structures. The structures are designed to have center wavelengths at 600 nm, so using the ellipsometrically-measured refractive index values of 2.03 for Ta_2O_5 and 1.46 for SiO_2, the ¼ wave thicknesses were 74 and 103 nm, respectively. The thickness of the protective layer was chosen to be equal to a full wavelength so that it does not affect the transmittance at the peak wavelength.

We simultaneously fabricated a structure that included only the 30 nm thick Ag layer and the protective coating. This reference film was deposited on 50 nm SiO_2 so that the dielectric environment surrounding the Ag film was identical with the ITFs.

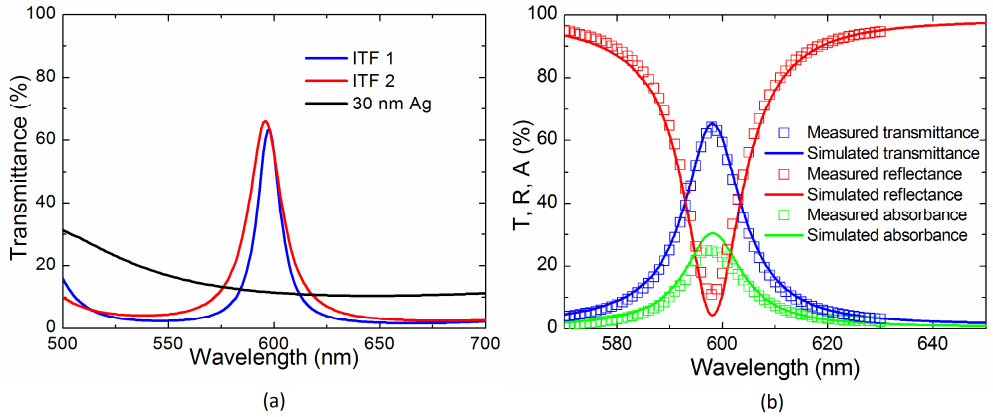

Fig. 3. (a) Measured transmittance of all three fabricated structures; (b) measured and simulated transmittance, reflectance, and absorbance of ITF 1.

Figure 3a shows the measured linear transmittance of all three structures, and Fig. 3b shows the measured transmittance and reflectance of ITF 1 compared with simulations. It can be seen that the ITF greatly enhances the transmittance of the Ag film over a narrow bandwidth.

The change in NLO response with time of the 30 nm Ag film is shown in Fig. 4, with a pump fluence of 32 J/m^2 and a probe wavelength of 600 nm. The first 0.7 ps is dominated by the instantaneous nonlinear response of the glass substrate. The remaining time shows the

#131590 - $15.00 USD Received 13 Jul 2010; revised 12 Aug 2010; accepted 14 Aug 2010; published 24 Aug 2010

initial strong response of the metal that can be attributed to an increase in the electron temperature, followed by a decay as the electrons cool down and the lattice heats up, as has been observed many times previously [21–27]. For the present study we are interested only in the initial strong response, particularly the moment after the substrate contribution has passed but before the electrons begin to cool down. To this end, all of the analysis in this section is performed at time t = 0.8 ps, as shown in the graph.

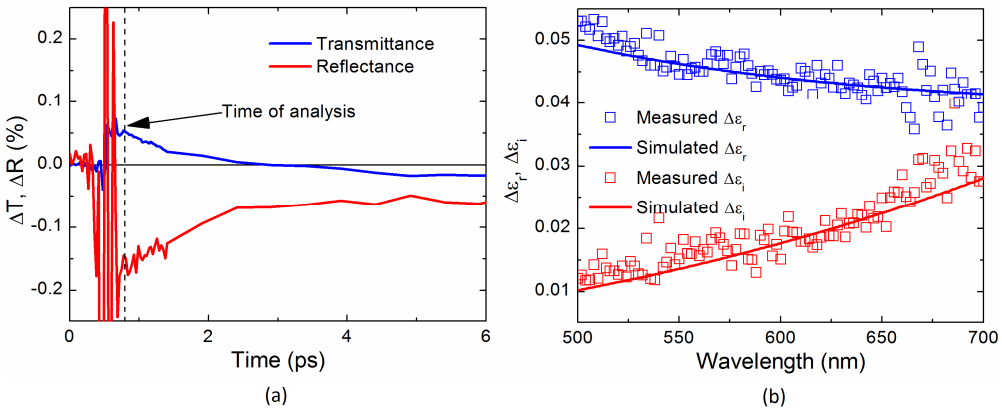

Fig. 4. (a) Measured temporal change in transmittance and reflectance of a 30 nm Ag film at 600 nm with a pump fluence of 32 J/m^2. (b) Measured and simulated spectral change in complex permittivity of the Ag film at 0.8 ps time delay.

The spectral response of the change in permittivity of the 30 nm Ag film at 0.8 ps is shown in Fig. 4b. This response was fitted to the electron temperature dependent Drude model parameter equations from [20]:

$$\varepsilon_\infty = 4 + 4.4\times10^{-8}\left(0.7 + 3\times10^{-32}\omega^2\right)T_e^2 \tag{8a}$$

$$\gamma = 7.97\times10^{13} + 2.9\times10^{6}T_e^2. \tag{8b}$$

These equations were developed for an Ag film that is only 20 nm thick; since the Drude parameters are to some extent thickness dependent, these equations are only an approximation for the 30 nm thick films studied here. However, as can be seen from Fig. 4b, the equations fit well with the NLO response of the isolated film. For this reason they will serve well as the basis for the analysis that follows.

It is important to note that the use of this physical model implies that the NLO response of Ag is not being treated as a $\chi^{(3)}$ nonlinearity, but rather a thermally driven change in the $\chi^{(1)}$ element of the permittivity.

#131590 - $15.00 USD Received 13 Jul 2010; revised 12 Aug 2010; accepted 14 Aug 2010; published 24 Aug 2010

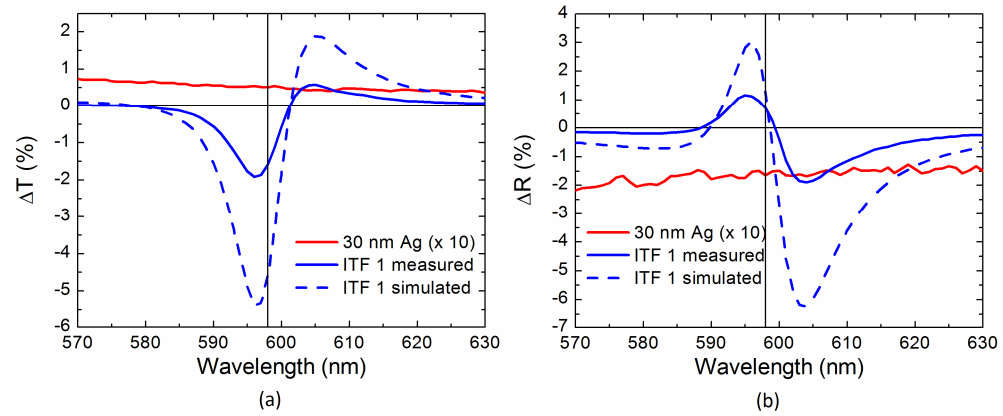

Fig. 5. Measured spectral changes in (a) transmittance and (b) reflectance of 30 nm Ag film and ITF 1, and simulated changes in ITF 1, at $t = 0.8$ ps due to 32 J/m^2 pump pulse at 600 nm.

Figure 5 shows the changes in transmittance and reflectance of ITF 1 due to a 32 J/m^2 pulse compared to the Ag film and a simulation based on Eqs. (2),8). The magnitude of the simulated response of ITF 1 is 90 times stronger than that of the 30 nm film and the magnitude of the measured response is 30 times stronger at the peak wavelength of the ITF transmittance, i.e. 598 nm. The behavior at this wavelength is noticeably different for the two films: whereas with the 30 nm film the transmittance increases and the reflectance decreases, the opposite is true with ITF 1. The large peak and valley indicates that the pass band of ITF 1 undergoes a red shift.

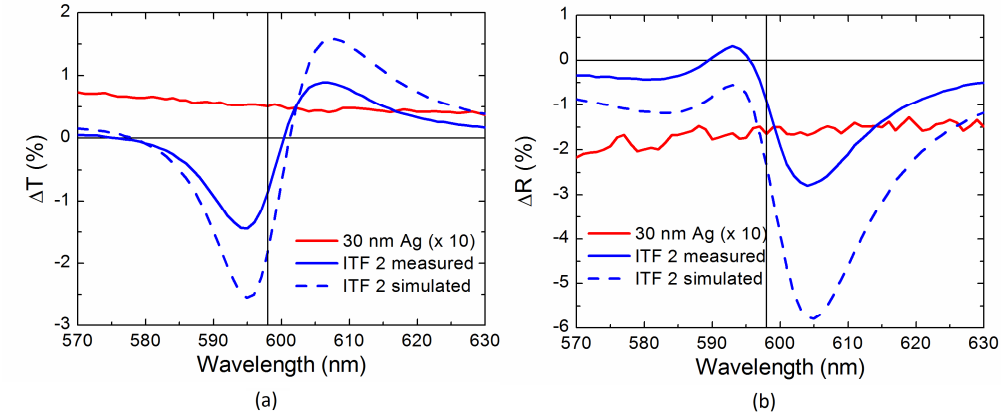

Fig. 6. Measured spectral changes in (a) transmittance and (b) reflectance of 30 nm Ag film and ITF 2, and simulated changes in ITF 2, at $t = 0.8$ ps due to 32 J/m^2 pump pulse at 600 nm.

Figure 6 shows the experimentally-determined NLO response of ITF 2, again compared to the data for the Ag film and to simulation. The general features are the same as ITF 1, except that there is a broad decrease in reflectance and the decrease in transmittance is not as strong. Still, the measured NLO response at the peak wavelength is 16 times that of the Ag film.

The simulated results of the NLO response of the ITFs match qualitatively well with the measured response. Quantitatively the measured ITFs fall short of the simulation; this could be for several reasons. The most likely reason is that the pump wavelength is not perfectly aligned with the peak of the ITF. A deviation of only a few nanometers can cut the response in half (or more) because the amount of energy absorbed by the Ag falls off rapidly with ITF linear transmittance. For instance, shifting the pump wavelength by 10 nm would decrease the change in transmittance of structure 1 at the peak from −4.6% to −1.8%. Error in Eqs. (7),(8)

#131590 - $15.00 USD Received 13 Jul 2010; revised 12 Aug 2010; accepted 14 Aug 2010; published 24 Aug 2010

also likely contributes to this discrepancy, and it is possible that there is some NLO contribution from the dielectric layers that may increase the error. Also, it is possible that morphology differences between the standalone Ag film and the Ag film in the ITF structure contribute to the error. Regardless, the magnitude of the response of ITF 1 is significantly higher than that of the isolated film at the peak wavelength.

There are two main reasons that the NLO responses of the ITFs are significantly stronger than that of the 30 nm Ag film. The first reason is that five to six times more energy is absorbed in the ITFs because of the resonance effects, so the change in electron temperature is greater. Thus, the intrinsic change in the permittivity is greater. The other reason is that spectral modulation effects such as the red shift come into play. In the remainder of this paper we discuss principles of ITF design and how the NLO response of an ITF can be optimized.

5. Discussion

5.1 Absorption and the NLO response

An important matter to consider when designing an ITF for NLO applications is the tradeoff between absorption and nonlinear response. Because the strong nonlinearity of the metal is thermal in origin, it is driven by absorption: all of the energy absorbed by the Ag film is converted to thermal energy in the electron cloud. This thermal energy, in turn, causes a change in the optical response. For this reason, absorption and nonlinearity are inextricably intertwined and attempting to minimize the absorption of a structure inevitably leads to a decrease in the nonlinear response. Thus, the goal for designing an ITF, or indeed any structure taking advantage of the thermally-induced optical nonlinearity of metal, is not to minimize the absorption but to make the best use of the absorption that is there.

With this in mind, it will prove useful to engineer an ITF to have an optimized absorbance. For example, if a structure has the design requirement that it must have at least 70% transmittance at the peak wavelength, assuming that the structure is an ideal ITF with no reflectance at the peak, then the remaining 30% of the light can be absorbed and contribute to the nonlinearity.

There are at least two ways of managing the absorbance of the ITF. The more obvious way is to adjust the thickness of the Ag film: a thicker film will have greater absorption. The alternative is to add a dielectric structure on the top side of the Ag film, turning a single sided ITF into a double sided ITF. Within the construct of the Fabry-Perot structure, this additional dielectric structure can be considered as part of the Ag mirror and will, depending on the design, either enhance or inhibit the reflections off the Ag film. If the reflectance of the Ag film is enhanced by the dielectric structure, the concentration of the electric field in the neighborhood of the Ag film within the ITF increases. This leads to an increase in absorbance in the Ag film. Thus, a thin Ag film with a top dielectric structure can absorb as much as a thicker Ag film without a top dielectric structure. The converse is true if the reflectance is inhibited; this is, in fact, the case in the original designs of Berning [16].

Thus, converting a single sided ITF to a double sided ITF greatly increases the flexibility of the design. Using these design guidelines it is possible, within certain limitations, to design an ITF with an arbitrary thickness of Ag giving arbitrary transmittance and absorbance at the peak wavelength.

5.2 Theoretical linear optical response of ITFs

Table 1 presents a series of examples of ITF designs that illustrate these design principles. Structures 1 through 3 are single sided, and structure 4 is double sided. The refractive indices n_l and n_h are constant across the spectral range of interest. Structure 1 is a perfectly matched structure, in which the refractive indices of the dielectric layers were chosen so that the reflectivity of the ¼ wave stack would match exactly with the 30 nm Ag layer and the spacer compensates exactly for the total interface phase shift.

#131590 - $15.00 USD Received 13 Jul 2010; revised 12 Aug 2010; accepted 14 Aug 2010; published 24 Aug 2010

Table 1. Structures of ITFs used for simulation

	ITF structure: G $(HL)_{x1}$ R_1 Ag R_2 $(LH)_{x2}$						
Structure	n_l	n_h	x_1	R_1 (nm)	Ag (nm)	R_2 (nm)	x_2
S1 (perfect match)	1.5	2.11	4	73.6	30	—	—
S2 (under-matched)	1.5	2.0	4	73.6	30	—	—
S3 (over-matched)	1.5	2.2	4	73.6	30	—	—
S4 (thin Ag)	1.5	2.11	4	69.7	15	55	2

As can be seen in the reflection spectrum shown in Fig. 7, the reflectance is zero at the peak wavelength. Structures 2 and 3 have the same design as structure 1, except that the refractive index of the high index material is varied. Structure 2 is under-matched (meaning the reflectance of the ¼ wave stack is less than the Ag film) because the refractive index of the high index material is slightly lower than from structure 1. Conversely, structure 3 is over-matched because the reflectance of the ¼ wave stack is greater than the Ag film. These two structures no longer have exactly zero reflectance at the peak wavelength, and the transmittance of each is slightly lower than structure 1. Structure 4, the double sided structure, makes use of a 15 nm Ag film where the reflection of the Ag has been augmented by the top side dielectric structure. The reflectance is designed to be zero at the peak wavelength, and the transmittance is slightly higher than structure 1.

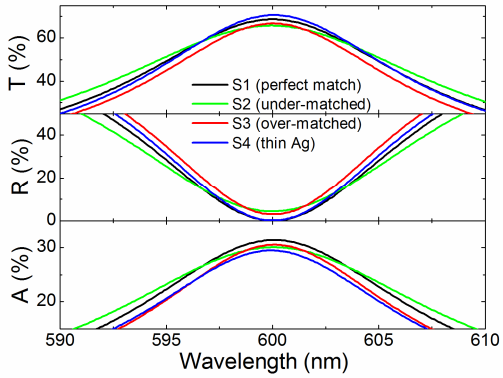

Fig. 7. Transmittance and reflectance of ITF structures 1-4.

Figure 8a shows the light intensity within structure 1 for a pump wavelength of 600 nm, and Fig. 8b shows the intensity within the Ag layer for structures 1-4 and an isolated 30 nm Ag film. All of the structures show significant enhancement over an isolated film. As expected, the enhancement in structure 4 is significantly larger than that of the other three.

#131590 - $15.00 USD Received 13 Jul 2010; revised 12 Aug 2010; accepted 14 Aug 2010; published 24 Aug 2010

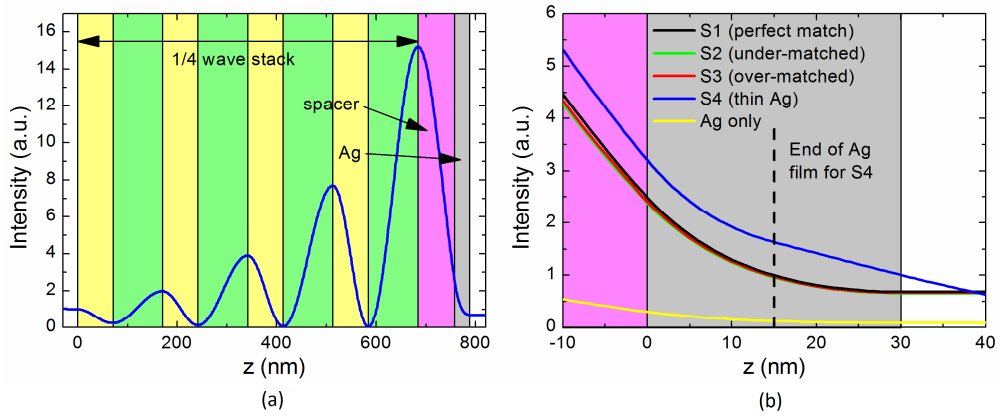

Fig. 8. (a) Intensity distribution of 600 nm wavelength within structure 1. (b) Intensity distribution of 600 nm wavelength in Ag layer of structures 1-4 and isolated Ag film.

5.3 Theoretical nonlinear optical response of ITFs

Figure 9a shows how the transmittance, reflectance, and absorbance of structure 1 change with increasing pump fluence, and Fig. 9b shows the changes in transmittance, reflectance, and absorbance of all four structures with a pump fluence of 50 J/m^2. Three mechanisms that contribute to the NLO response of an ITF can be gleaned from these simulations. They are the (1) nonlinear phase shift within the cavity, (2) nonlinear absorption in the Ag film, and (3) nonlinear reflection of the structure.

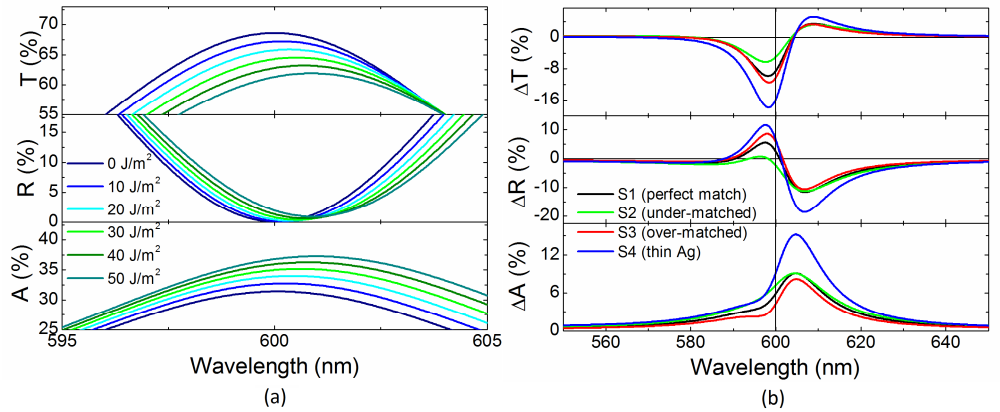

Fig. 9. (a) Transmittance, reflectance, and absorbance of structure 1 under illumination by pump pulses at 600 nm with powers ranging from 0 to 50 J/m^2. (b) Changes in transmittance, reflectance, and absorbance of structures 1-4 due to a 50 J/m^2 pump pulse.

First, a red shift can be observed in the peaks of all of the structures. This shift, as described in the experimental section, is responsible for the peak and valley formation seen in the changes in transmittance and reflectance. The red shift arises to compensate for the change in phase of the reflection off the Ag film. The peak wavelength is located at the point where the round trip phase shift within the cavity is an integer multiple of 2π; that is,

$$\Phi_{Ag} + \Phi_D + 2 \times \Phi_S = 2\pi n, \qquad (9)$$

where Φ_{Ag} is the phase shift of the reflection off the Ag film, Φ_D is the phase shift of the reflection off the dielectric mirror, Φ_S is the phase shift within the spacer, and n is an integer.

#131590 - $15.00 USD Received 13 Jul 2010; revised 12 Aug 2010; accepted 14 Aug 2010; published 24 Aug 2010

As the phase shift in the Ag film changes, the peak wavelength shifts to maintain zero round trip phase. The shift in the peak wavelength, $d\lambda$, can be calculated using the equation

$$\Phi_{Ag\ NL} + d\lambda\left(\frac{\partial\Phi_{Ag}}{\partial\lambda} + \frac{\partial\Phi_{D}}{\partial\lambda} + 2\times\frac{\partial\Phi_{S}}{\partial\lambda}\right) = 0, \qquad (10)$$

where $\Phi_{Ag\ NL}$ is the nonlinear phase shift in the Ag film, and is always negative. The three differential terms are all positive, so $d\lambda$ is positive, representing a red shift in the transmission peak. The strength of this phase shift is similar across all of the structures.

Second, the observed nonlinear absorption arises from the fact that as the Ag film is heated by the incident pulse it becomes more absorptive. This effect results in a decrease in transmittance across the spectrum of the ITF. This effect contributes approximately equally to the changes in structures 1-3, and is 1.9 times as strong in structure 4. The greater response in structure 4 is caused by the fact that the average intensity within the Ag film of structure 4 is about twice the average intensity in the other structures. The nonlinear absorption is proportional to the average intensity in the Ag film. However, this enhancement comes at the cost of increasing the complexity of the structure.

Third, a nonlinear reflection component can be observed. This effect can be seen in Fig. 9a; as the pump fluence increases, the reflectance at the peak also increases. This effect is a function of how well the reflectance of the ¼ wave stack matches the Ag film, and is the primary cause of the difference in response among structures 1-3. As the Ag film heats up, it becomes less reflective; this changes how well the Ag film matches the ¼ wave stack. If the linear reflectance of the ¼ wave stack is less than the Ag, then the two mirrors will end up more closely matched as the Ag film heats up. This leads to a decrease in the reflectance of the full structure and a corresponding increase of the transmittance as seen in Fig. 9b. If, on the other hand, the ¼ wave stack is more reflective than the Ag, then the matching will get worse, the reflectance will increase, and the transmittance will decrease.

The effects of nonlinear reflection either offset or enhance the effects of nonlinear absorption, as can be seen from the responses of the under-matched and over-matched structures, respectively. Thus, the total change in transmittance will be greatest for structures that are somewhat over-matched. The enhancement of nonlinear transmittance for the simulated over-matched structure (structure 3) with respect to a perfectly matched structure (structure 1) at the peak wavelength is 1.2. This enhancement is a function of how far over-matched the structure is; if the mismatch is increased this enhancement may increase, but at the cost of decreased linear transmittance and increased linear reflectance.

The change in nonlinear transmittance, therefore, can be achieved with a double sided structure that has a minimum thickness of Ag and is slightly over-matched. To illustrate this scenario, Fig. 10 shows the changes in transmittance and reflectance for a structure of the form

$$G\ (H_1L)_4\ R_1\ Ag\ R_2\ (LH_2)_2, \qquad (11)$$

where $n_{h1} = 2.2$ and $n_{h2} = 2.109$. The thickness of Ag is 15 nm and the spacer thicknesses are 69.7 and 55 nm, respectively, the same as structure 4 above. Also shown for comparison are the responses of the perfectly matched structure and the thin Ag structure (structures 1 and 4). The change in transmittance of this optimized ITF is larger than that of structure 1 by a factor of 2.3 at the peak wavelength.

#131590 - $15.00 USD Received 13 Jul 2010; revised 12 Aug 2010; accepted 14 Aug 2010; published 24 Aug 2010

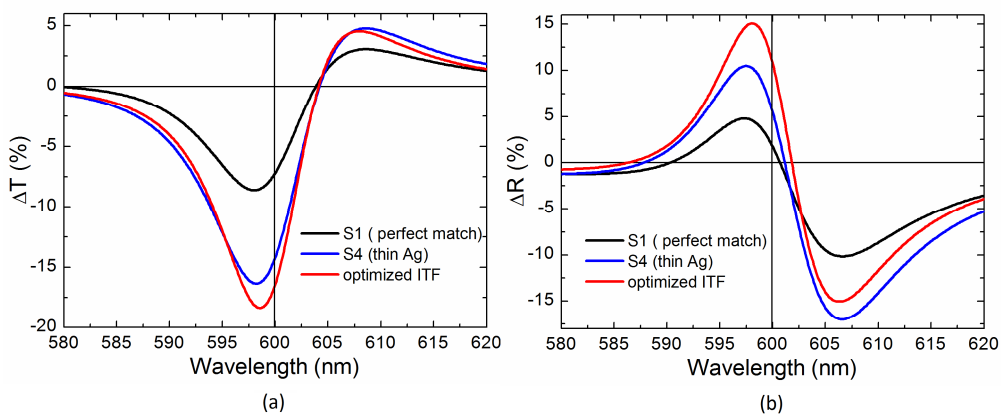

Fig. 10. Changes in transmittance and absorbance for an optimized double-sided ITF structure compared to structures 1 and 4 due to a 50 J/m^2 pump pulse.

6. Conclusion

We have investigated, by experiment and simulation, the NLO properties of ITFs. We demonstrated the amplification of the NLO response of an ITF by a factor of 30 over an isolated Ag film using white-light continuum pump-probe measurements. Through simulation, we also explored the effects of variations in design parameters, specifically the thickness of the Ag film and the relative reflectances of the dielectric structure and the Ag film, on the magnitude of the NLO response of the ITF. We found that the NLO response can be broken down into three contributions (namely nonlinear absorption, nonlinear reflection, and a nonlinear phase shift), and that over-matched structures exploit these contributions the best to produce the greatest change in nonlinear transmittance. Also, thinner Ag films lead to stronger changes of the NLO response. Although the changes in transmittance shown here are relatively small, the enhancement of the NLO response provided by such structures could be very attractive for the nonlinear control of laser fluence if metals with a stronger NLO response than Ag, such as Au, are used instead.

Acknowledgements

We would like to thank Prof. Seth Marder and his group for the use of their spectrophotometer. This work was partially funded by NSF through STC-DMR-0120967, by ARO through contract/ grant 50372-CH-MUR, by AFOSR (BIONIC Center grant No. FA9550-09-1-0162), and AFOSR (grant No. FA9550-09-1-0418).

#131590 - $15.00 USD Received 13 Jul 2010; revised 12 Aug 2010; accepted 14 Aug 2010; published 24 Aug 2010